The Constitution and Phase Stability of Overlapping Melt Trails in Ag-Cu Alloys Produced by Continuous Laser Melt Quenching

DAVID G. BECK, STEPHEN M. COPLEY, and MICHAEL BASS

Coatings consisting of overlapping trails melted with a scanning CW CO_2 laser have been produced on Ag-Cu alloys with the following compositions: Cu 17 at. pct Ag; Cu 37 at. pct Ag; Cu 61.7 at. pct Ag; Cu 71.8 at. pct Ag; and Cu 82 at. pct Ag. The laser beam was scanned at a velocity of 34 cm s^{-1} and with an intensity of 3.6 MW cm^{-2}. Selected trails were examined by X-ray diffractometry, optical microscopy, and scanning electron microscopy in the as-irradiated condition and after annealing for various periods of time in the temperature range 100 to 450 ° C. Time-temperature-transformation diagrams based on the annealing studies are presented. Significant amounts of the metastable extended solid solution (γ) were observed in the Ag-rich alloy trails. The silver rich terminal solid solution (α) was also detected, formed probably by solid state precipitation. An α' phase with lattice parameter lying between that of γ and α was also observed in the Cu 61.7 at. pct Ag alloy. A metastable equilibrium diagram has been constructed and is employed to interpret these observations. The most striking microstructural feature of the trails are bands marking sequential positions of the melt-solid interface. We propose that these bands are evidence for planar, oscillating-steady-state, interface motion. The observation of a periodic cellular breakdown of the planar interface in the Cu 61.7 at. pct Ag alloy is attributed to a diffusional instability previously predicted by Baker and Cahn.

I. INTRODUCTION

SOLIDIFICATION of undercooled melts is a well established method for synthesizing metastable phases. Two approaches, generally, have been employed to produce undercooled melts, rapid quenching, and nucleant isolation. In rapid quenching, large undercoolings can be attained in the melt prior to nucleation of the solid phase. Also, kinetic undercooling at the interface may occur due to the high solidification rates. In nucleant isolation, high undercooling results from dispersing the sample into fine droplets within an inert carrier fluid, thus isolating the active nucleation catalysts.

Previous investigations of the solidification of undercooled Ag-Cu alloys have employed the rapid quenching approach. Duwez *et al*[1] and others[2–6] employed "splat cooling," a technique in which a small volume of melt is quenched by flattening it against a massive heat sink. Elliot *et al*[7] employed a pulsed Nd-glass laser to melt small volumes at the surfaces of their samples. In this case, the sample serves as: a heat sink; a seed for crystallization of the equilibrium phases; and, a possible catalyst for nucleation of metastable phases. In both the splat cooling and pulsed laser quenching experiments, kinetic undercooling probably occurs due to the high but variable solidification rates.

In our investigation of the solidification of undercooled melts of Ag-Cu alloys, a small volume of material at the surface of the specimen is continuously melted and resolidified by moving the specimen at a constant speed under the beam of a CW CO_2 laser. The sample serves the same purposes as in the pulsed laser experiments; however, in contrast to the pulsed laser and splat cooling experiments, solidification occurs at a constant rate. The solidification rate, amount of kinetic undercooling, and the melt and solid compositions at a specific position on the melt-solid interface are determined by the speed at which the specimen is moved under the beam, the laser power, and the substrate temperature.

In most conventional casting processes, kinetic undercooling is only a few hundredths of a degree. If, however, the solidification rate is sufficiently high, the amount of kinetic undercooling may be large. Consider, for example, the coupled eutectic growth of a Cu 50 at. pct Ag alloy. According to Tiller, the amount of undercooling required for a specific solidification rate is plotted in Figure 1 (see Appendix VI-A for details of the calculation).[8] Although the plot should be regarded as approximate, it indicates undercooling increases markedly with increasing solidification

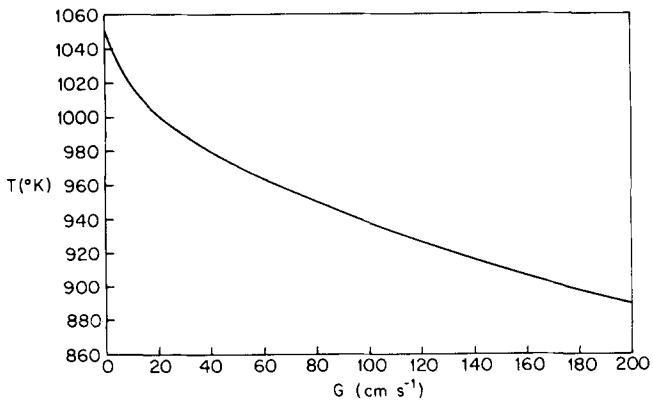

Fig. 1 — Growth rate *vs* melt temperature.

DAVID G. BECK is Research Assistant, Department of Materials Science, STEPHEN M. COPLEY is Professor, Departments of Materials Science and Mechanical Engineering, and MICHAEL BASS is Professor, Department of Electrical Engineering and Director, Center for Laser Studies. All are with the University of Southern California, University Park, Los Angeles, CA 90007.

Manuscript submitted November 25, 1981.

ISSN 0360-2133/82/1111-1879$00.75/0

rate; also, undercoolings of 10 to 100 K can be attained at the speeds employed in CW laser melting experiments. Such undercoolings may be sufficient to allow replacement of the coupled eutectic-melt interface with a metastable solid-melt interface, which might require less undercooling to move at the imposed speed. Indeed, we have previously reported detection of the metastable extended solid solution in single continuous melt trails of Ag-Cu alloys melted at a specimen speed of 10 cm s^{-1}.[9]

The purpose of this investigation was to determine the constitution and phase stability of overlapping melt trails in Ag-Cu alloys. It was anticipated that a surface coating consisting of overlapping melt trails would give much greater diffracted intensity than the single trails previously studied making possible a more complete determination of the as-irradiated constitution, and also the annealing response. Such information is essential to evaluate the feasibility of employing continuous laser melt quenching to produce metastable surface coatings or, in combination with a suitable deposition process, to produce metastable bulk alloys.

II. EXPERIMENTAL PROCEDURE

A. *Sample Preparation and Laser Irradiation*

Five compositions of the Ag-Cu alloy system were chosen for this experiment: Cu 17 at. pct Ag, Cu 37 at. pct Ag, Cu 60 at. pct Ag, Cu 70 at. pct Ag, and Cu 82 at. pct Ag. Table I gives the chemical analysis for representative samples from the Cu 60 and Cu 70 at. pct Ag alloys. Detailed analyses were carried out because most of the data was obtained from these alloys.

The five alloys were formed from 99.99 pct pure copper and 99.999 pct pure silver and repeatedly mixed with an arc button melter to promote homogenization. An observation from earlier work was that the coarsened and spheroidized microstructure of the parent matrix made mixing difficult during the short melt times characteristic of laser melt quenching. Two precautions to avoid incomplete mixing were therefore taken in the current investigation: (1) a very fine microstructure was produced in the parent matrix and (2) the surface was laser treated prior to the actual experiment.

To achieve a fine microstructure, each alloy sample, in the form of a 100 gm bar, was placed in a quartz tube inside of a verticle furnace. It was held at a temperature approximately 45 °C above its melting point in an argon atmosphere for two hours and then was drop quenched into a water bath.

After the above melting and quenching process, each sample was a 15 mm diameter rod. Two millimeter thick specimens were cut from the rods using a high speed, low translation rate wafering saw. The samples were polished down to 180 grit paper, a rough finish being preferred to a highly polished surface to help the adherence of the absorption enhancing coating. The coating, a 50/50 mix of 44 μm graphite flakes and isopropanol, was then applied.

Table I. Chemical Analysis of the Cu 60 At. Pct Ag and Cu 70 At. Pct Ag Samples

	Cu 60 At. Pct Ag			Cu 70 At. Pct Ag		
	Anal. #1	Anal. #2	AVR	Anal. #1	Anal. #2	AVR
Cu (at. pct)	38.29	38.24	38.3	29.30	27.19	28.2
Ag (at. pct)	61.71	61.77	61.7	70.70	72.81	71.8

As previously stated, to obtain a finely mixed surface layer, each sample was laser treated prior to the actual experiment. In this treatment, overlapping melt trails were produced by scanning the samples at a rate of 8 cm s^{-1} with a trail spacing of 59 μm. The samples were then mechanically polished with 400 grit paper and coated once again with the graphite absorption enhancing coating. This initial treatment left a nearly smooth surface with a highly mixed, ultrafine microstructure for a surface layer, an ideal base structure from which to laser quench the metastable phase.

The second set of trails was scanned at a rate of 34 cm s^{-1}, with a trail spacing of 39 μm. These trails were scanned parallel to the first set of trails. Figure 2 shows a laser melt trail, scanned at 34 cm s^{-1}, which lies partially on a laser pretreated region and partially on a region with the fine microstructural characteristics of the bulk material. It is obvious that the microstructure of the bulk material is not fine enough to insure compositional homogeneity in a trail melted at 34 cm s^{-1} even though evidence of strong convection (swirls) can be seen. Thus, laser pretreatment appears to be necessary to obtain complete dissolution and mixing in trails of Ag-Cu alloys melted at high velocities.

The laser, operating at a wavelength of 10.6 μm, had an output power of 1350 W and an incident power of 1090 W. To determine accurately the mode as well as the focussed beam diameter, beam scanning techniques were applied. Figure 3 shows two of the central beam scans, situated at 90 degrees to one another, with Gaussian overlays. Using this information the laser's mode was calculated to be approximately 94 pct Gaussian (TEM_{00}) at the time of the experiment. A $1/e^2$ focussed beam diameter of 196 μm was determined, yielding an average power density of 3.6 MW cm^{-2}. The samples were clamped to a rotating stage that was translated under the beam to produce overlapping trails. A conductive paste was used to improve heat transfer from the sample to the stage. To prevent oxidation reactions from occurring during irradiation, the samples were covered with an inert atmosphere during scanning. The laser beam was oriented at normal incidence to the samples.

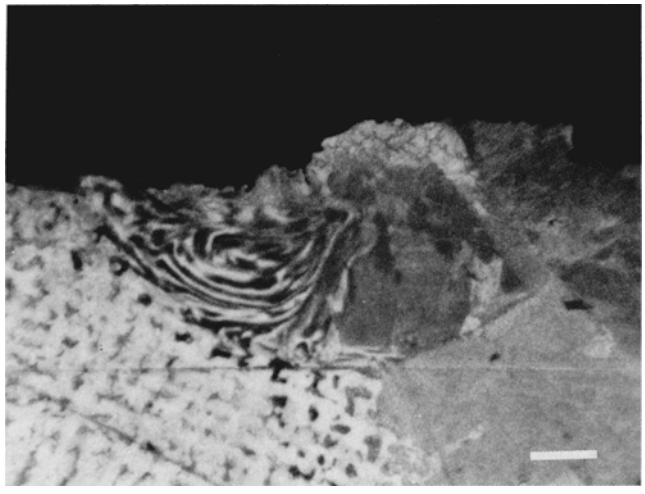

Fig. 2—A melt trail lying half on the untreated parent matrix and half on the laser treated area (marker indicates 7.5 μm).

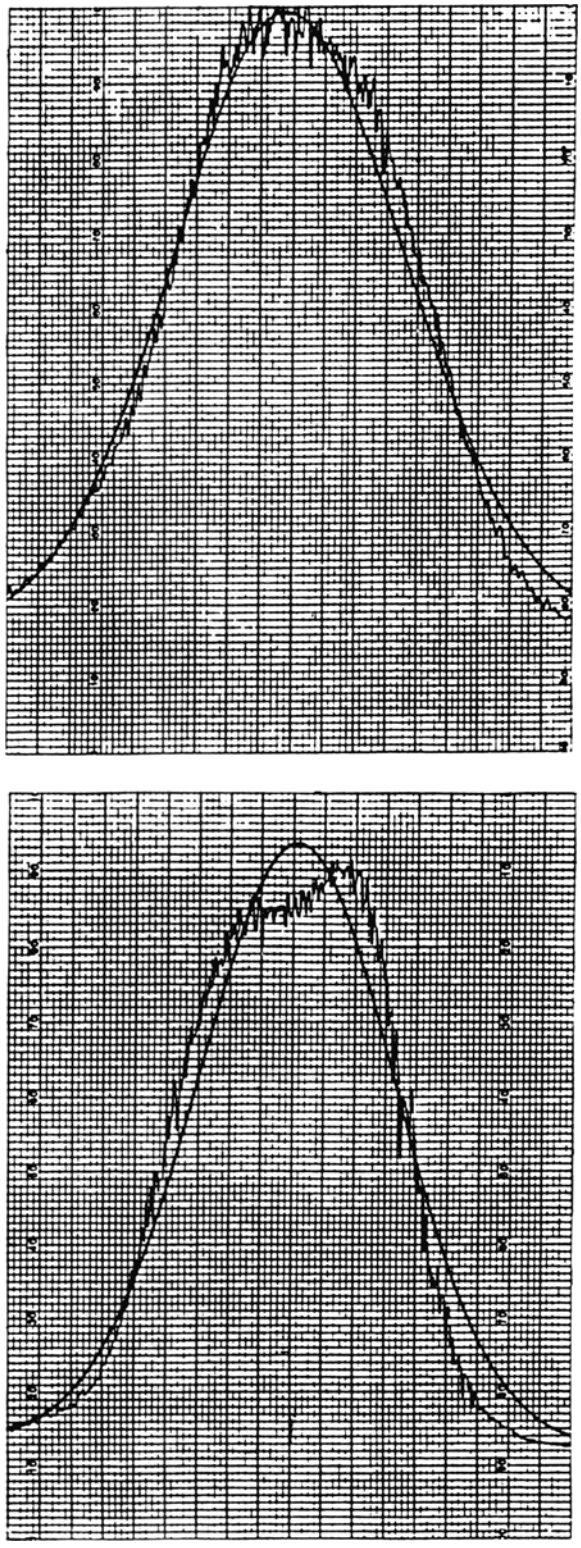

Fig. 3—Actual beam scans, oriented at 90 deg to one another, with Gaussian overlays.

B. *X-Ray Analysis*

An X-ray scanning diffractometer was employed in this study to analyze the specimens. The main problem encountered in this analysis related to the intensity of the diffracted peaks. Unfortunately, the intensity of the diffracted beams for both silver and copper is small. Further complications arose due to the surface topography of the samples. Since the samples were repeatedly scanned with a laser beam, their surfaces are comprised of a series of alternating crests and troughs. The amount of height difference can be reduced prior to the sample's insertion into the diffractometer by very light polishing; however, because the treated material in the surface is the material of interest, only a small amount may be polished off, leaving a surface which is still made up of troughs and modified crests. This variation in surface height results in the broadening of the diffracted peaks and thus a further lowering of the peak intensity. Peak broadening, with its resultant loss in peak intensity, may also arise from compositional inhomogeneity.

Two solutions to the problem of low diffraction intensity were applied. First, large angle incident beam slits and receiving slits were used. Although this reduced the peak resolution, it was necessary in order to gain sufficient diffracted intensity. Second, no filter was employed on the copper tube. This meant the addition of a very small CuK_β peak, but it allowed the incident intensity, and thus the diffracted intensity, to be greater.

C. *Annealing Study*

In this investigation only the Cu 61.7 at. pct Ag and the Cu 71.8 at. pct Ag specimens were studied. Four temperatures between 100 °C and 450 °C were selected. Commercially available annealing salts were used for the three highest temperatures and boiling distilled water for the lowest. To obtain accurate values for both the annealing time and temperature, thermocouples were attached to the specimen holder, therefore allowing both values to be recorded simultaneously. The specimens were quenched in water which was at room temperature.

Phase changes were observed through X-ray scanning diffractometry. X-ray peak intensities were recorded at various annealing times. Unfortunately, these intensities give only a qualitative measure of the extent of the phase change. Obviously, experimental details such as sample positioning in the diffractometer are quite critical in order to obtain consistent values.

III. RESULTS

Figures 4(a-e) are typical X-ray patterns for the (111) set of reflections for each composition. The counts per second (CPS) range, noted individually on each X-ray pattern, were varied in order to optimize resolution.

Those samples that contained 61.7 at. pct Ag or more all showed evidence of the metastable γ phase. The lattice parameters of the γ phase for the three Ag-rich alloys are plotted in Figure 5 along with Duwez's results on the lattice parameters of nonequilibrium solid solutions in Ag-Cu alloys formed by splat cooling.[1] Data taken in an earlier study of single melt trails[9] are also plotted in Figure 5.

In the samples containing 61.7 at. pct Ag or more, the terminal silver α phase was also observed; however, only in the Cu 61.7 at. pct Ag specimen was the terminal copper phase detected. In this same composition, an additional peak was observed. This phase, designated α' in Figure 4, had a broad peak lying between the α and γ peaks. In both alloys containing less than 61.7 at. pct Ag, there was no

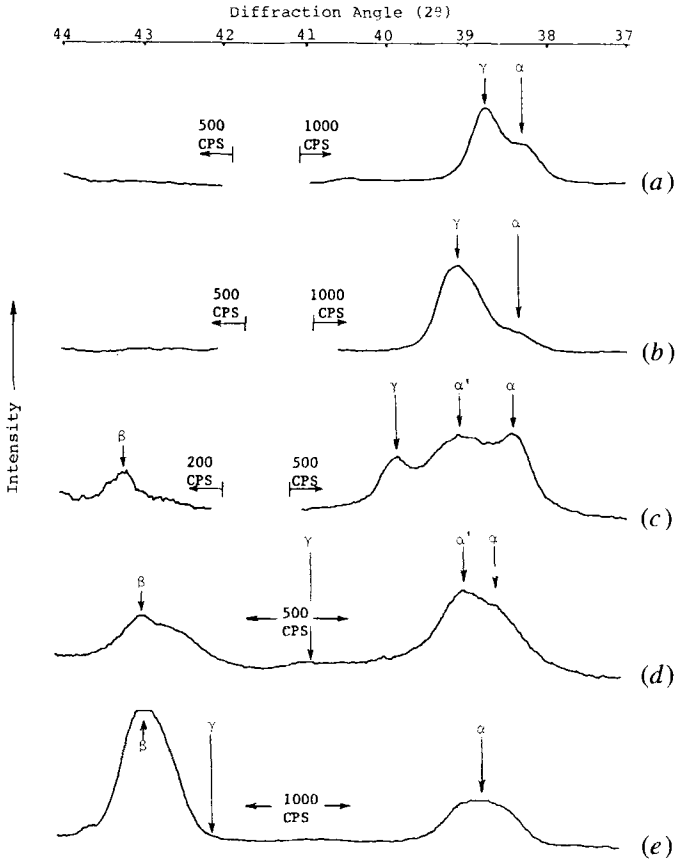

Fig. 4—Typical X-ray patterns for the (111) reflection in (*a*) Cu 82 at. pct Ag, (*b*) Cu 71.8 at. pct Ag, (*c*) Cu 61.7 at. pct Ag, (*d*) Cu 37 at. pct Ag, and (*e*) Cu 17 at. pct Ag (CPS range as noted).

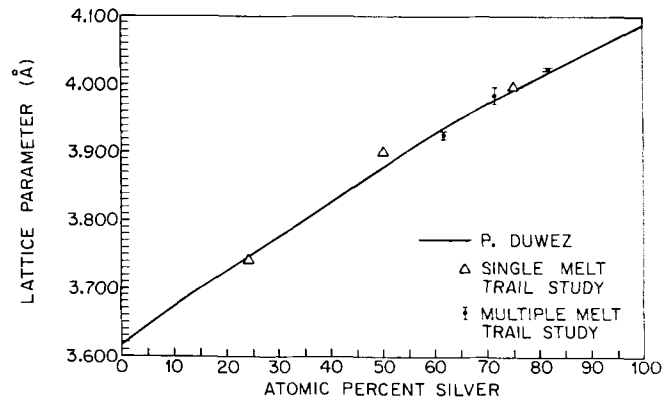

Fig. 5—A comparison of metastable phase lattice parameters found by (i) Duwez using splat cooling, (ii) single melt trails, and (iii) multiple melt trails.

indication of a metastable phase; however, in both samples, the α and β peaks showed slightly extended terminal solid solubilities.

Table II lists each alloy with the lattice parameters of the resolvable phases. Whenever possible, tolerances are given.

Figures 6 and 7 each show a family of diffraction curves, illustrating how the annealing data were taken. Figure 6 shows the (111) reflection for a Cu 61.7 at. pct Ag sample while Figure 7 shows the same reflection in a Cu 71.8 at. pct Ag sample. In both figures, as the annealing time is increased, the γ peak disappears while the α peak grows. In the Cu 61.7 at. pct Ag alloy, no shift in lattice parameter was detected during growth of the α peak. Figure 6 also shows the α' peak slowly decreases in intensity. The results of the annealing studies are summarized in Figures 8 to 10, which give TTT (Time-Temperature-Transformation) curves for the γ phase for the Cu 71.8 at. pct Ag and Cu 61.7 at. pct Ag alloys as well as the α' phase for the Cu 61.7 at. pct Ag sample. In these diagrams, the pct transformed reported is based on the pct change in diffraction peak height.

A careful examination of melt trails in the Cu 71.8 at. pct Ag and Cu 61.7 at. pct Ag specimens revealed only occasional and isolated instances of cellular solidification. The most striking microstructural features of the melt trails are regularly spaced bands that appear to mark sequential positions of the melt-solid interface. We have previously observed similar bands in Cu 25 at. pct Ag, Cu 50 at. pct Ag, and Cu 75 at. pct Ag alloys and showed that they corresponded to variations in Cu concentration of at least 1.1 at. pct.[9] Figure 11 shows micrographs taken of the cross sections of annealed trails for the Cu 61.7 at. pct Ag and Cu 71.8 at. pct Ag specimens. These were the same specimens used to obtain the data upon which Figures 6 and 7 were based. The inset in each micrograph was taken from a sample with the same composition but in the as-laser-melted, unannealed state. The alignment of the bands, most evident in the inset, and the lack of other features in the melt trails of the Cu 71.8 at. pct Ag alloy suggest that it solidified with a planar interface. The disruption of bands apparent in micrograph Figure 11(b) occurred only at the surface. In the Cu 61.7 at. pct Ag alloy, the bands in the as-laser-quenched unannealed state appear similar to those in the Cu 71.8 at. pct Ag alloy. In the annealed state, however, the bands appear to be a series of sharp dark lines. At higher magnification each dark line appears to be a row of small precipitate particles aligned perpendicular to the band (Figure 12). The arrangement of particles in the rows suggests that they mark regions where a breakdown from a planar to a cellular interface might have occurred.

Table II. Lattice Parameters of Resolvable Phases

		a(Å)			
		α	β	γ	α'
Alloy	Cu 17 at. pct Ag	4.018	3.647	—	—
	Cu 37 at. pct Ag	4.005	3.647	—	—
	Cu 61.7 at. pct Ag	4.065 ± 0.007	3.628 ± 0.001	3.923 ± 0.006	3.990 ± 0.005
	Cu 71.8 at. pct Ag	4.061 ± 0.013	—	3.985 ± 0.011	—
	Cu 82 at. pct Ag	4.070 ± 0.006	—	4.026 ± 0.002	—

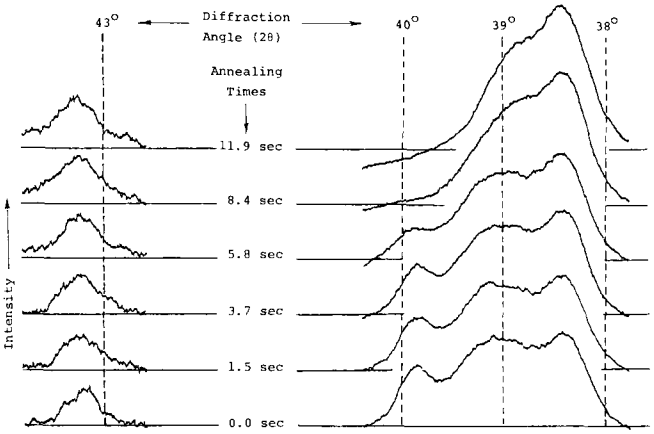

Fig. 6 — A 'family' of annealing diffraction curves for a Cu 61.7 at. pct Ag sample at a temperature of 420 °C. The horizontal lines are reference lines for comparing the intensities of the X-ray diffraction patterns.

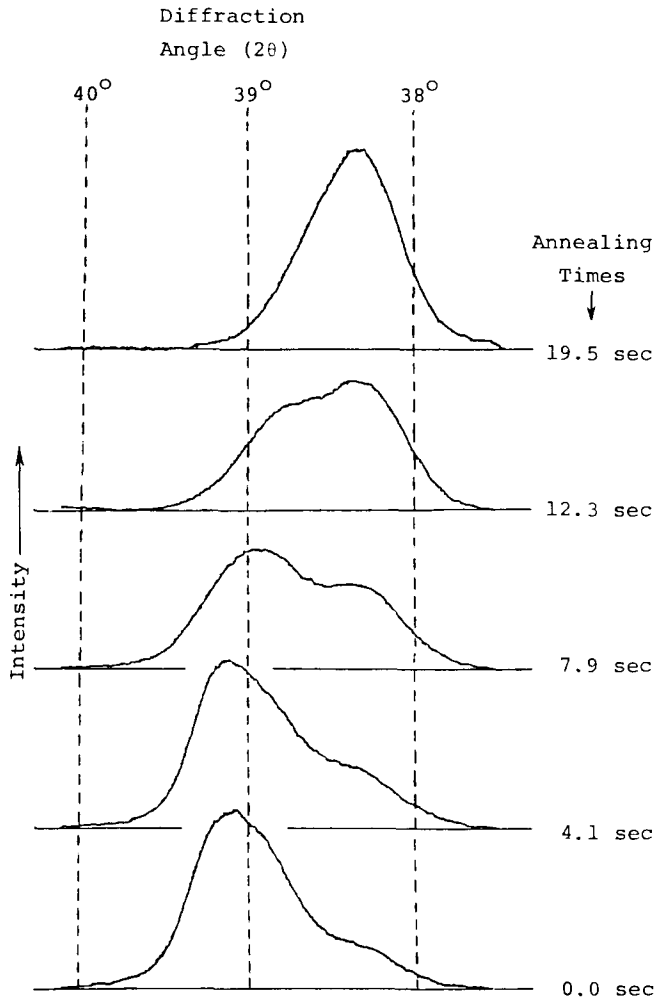

Fig. 7 — A 'family' of annealing diffraction curves for a Cu 71.8 at. pct Ag sample at a temperature of 420 °C. The horizontal lines are reference lines for comparing the intensities of the X-ray diffraction patterns.

IV. DISCUSSION

A. *Constitution of Laser Melted Trails*

The results for the Cu 71.8 at. pct Ag alloy demonstrate the feasibility of producing a coating consisting primarily of the metastable extended solid solution (γ) in Ag-Cu alloys by continuous laser melt quenching. Of course, some spinodal decomposition may have occurred, which would not have been detected by our X-ray technique; however, only a small amount of α was detected in the coating. Our results suggest that α precipitated during the repeated thermal cycles associated with overlapping of the melt trails. The annealing studies show α precipitation in γ occurs very rapidly; complete conversion of γ to the terminal solid solutions was observed to take place in 19.5 seconds at 450 °C. Also, according to Figure 5, the lattice parameter of α in Cu 71.8 at. pct Ag corresponds to a Cu fraction less than the maximum solid solubility limit of Cu in Ag, as would be expected if α resulted from solid-state precipitation.

Melt trails in the Cu 82 at. pct Ag and Cu 61.7 at. pct Ag alloys were found to contain large amounts of γ along with

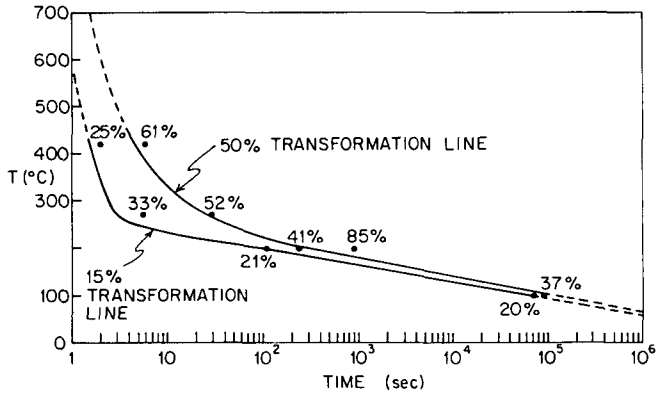

Fig. 8 — TTT diagram (γ transformation) for a Cu 61.7 at. pct Ag sample.

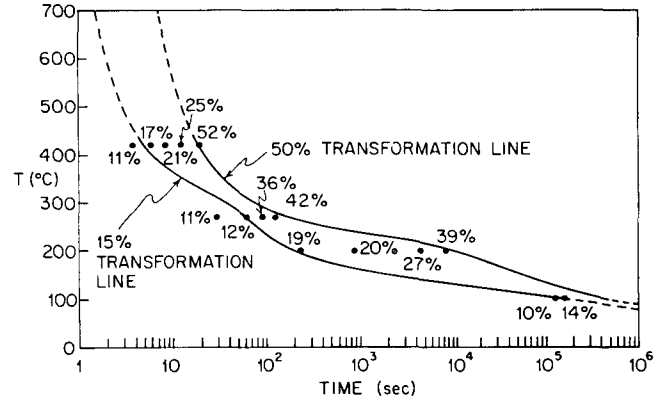

Fig. 9 — TTT diagram (α' transformation) for a Cu 61.7 at. pct Ag sample.

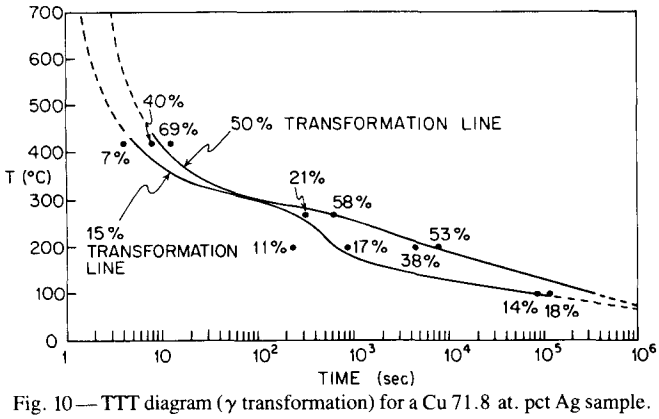

Fig. 10 — TTT diagram (γ transformation) for a Cu 71.8 at. pct Ag sample.

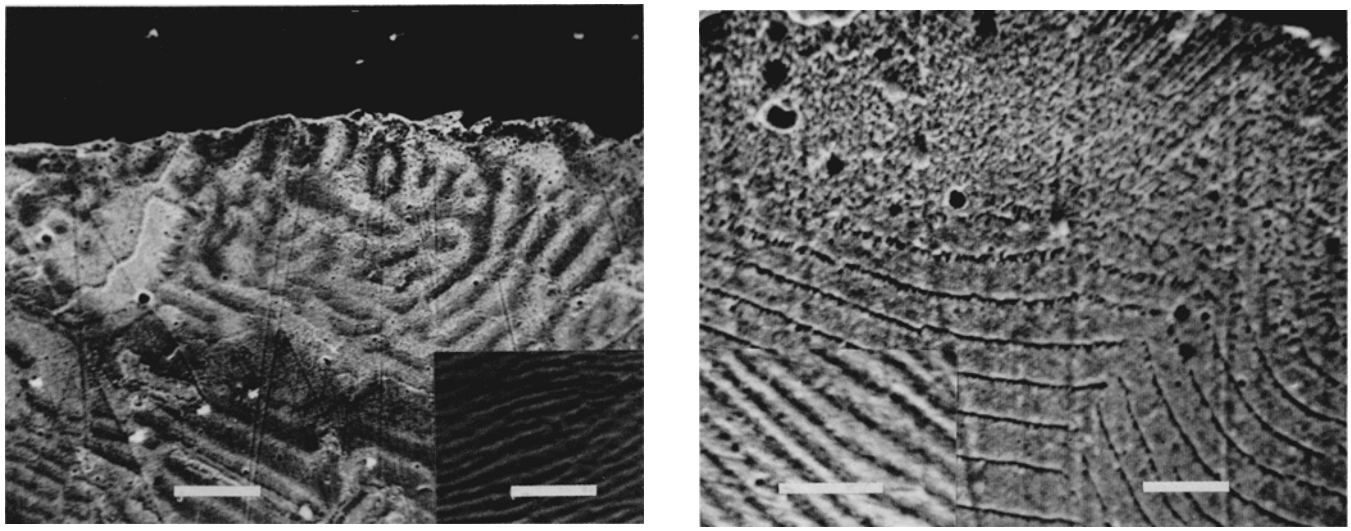

(*a*) (*b*)

Fig. 11 — Annealed banding structure with inset showing unannealed bands for a (*a*) Cu 71.8 at. pct Ag sample (markers indicate 5 μm) and a (*b*) Cu 61.7 at. pct Ag sample. Each micrograph and its inset were taken from different regions of different trails and thus show bands that differ in spacing and shape (markers indicate 2 μm).

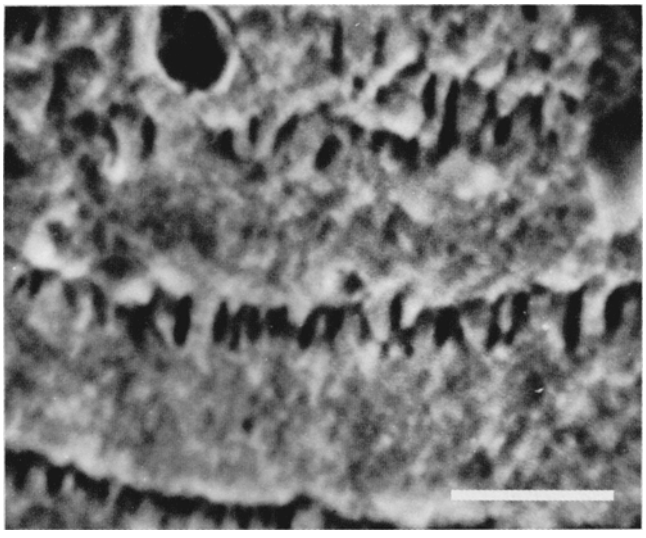

Fig. 12 — Annealed bands in a Cu 61.7 at. pct Ag sample (marker indicates 1 μm).

somewhat larger amounts of α than were found in the Cu 71.8 at. pct Ag alloy. The lattice parameters of the α phases in these alloys were similar to that of the Cu 71.8 at. pct Ag alloy suggesting that they too formed by solid state precipitation. It is not known whether the different amounts of α found in the three compositions are indicative of different degrees of stability for the metastable solid solution or differences in the annealing treatment associated with overlapping of the melt trails. A broad α' peak was observed in the Cu 61.7 at. pct Ag alloy with a lattice parameter less than that for α but greater than that for γ.

Melt trails in the Cu 37 at. pct Ag and Cu 17 at. pct Ag alloys did not contain detectable amounts of γ. Their X-ray patterns consisted of broad peaks corresponding to the terminal α and β solid solutions. The absence of γ in the coatings on the Cu 37 at. pct Ag and Cu 17 at. pct Ag alloys may be due to solid state precipitation of α and β. Other possible explanations are that (i) formation of γ was precluded thermodynamically because of insufficient undercooling, (ii) nucleation of γ is difficult, or (iii) the melt-γ interface was less mobile than the melt α/β interface at the interface temperature determined by the scan velocity (34 cm s^{-1}).

In order to interpret our results further, the metastable phase diagram shown in Figure 13 was constructed. This diagram is based on molar free energy curves for the solid calculated from the Ag-Cu equilibrium diagram using the Lumsden model.[10] It has been shown by Sundquist[11] that this model gives a good representation of the molar free energy curves for binary systems with a miscibility gap. Molar free energy curves for the melt are based on the extrapolation of established thermodynamic data. Details of the calculations are given in Appendix VI-B. The line labeled T_0 indicates the minimum undercooling necessary to solidify the metastable extended solid solution. Also shown are metastable solidus and liquidus lines.

The broad α' peak observed in the Cu 61.7 at. pct Ag alloy probably results from eutectic growth. According to Figure 13, metastable equilibrium exists between the liquid phase and an Ag-rich solid solution phase with a composition in the range of α'. At 700 °C, for example, the composition of the solid solution phase in metastable equilibrium with the liquid phase is Cu 82.9 at. pct Ag. The composition of the α' phase, estimated from its lattice parameter using Figure 5 is Cu 77 at. pct Ag. At high solidification rates, however, it is likely that the Ag-rich phase formed by eutectic solidification will contain greater than the metastable equilibrium amount of Cu so that identification of the α' phase as the Ag-rich eutectic phase is reasonable. It is likely that a similar distribution of phases exists as that observed in our previous investigation of single trails in a Cu 50 at. pct Ag alloy. Near the bottom of the trails we observed regions containing eutectic surrounded by regions that by their annealing response were identified as being metastable extended solid solution. It is not surprising to find regions

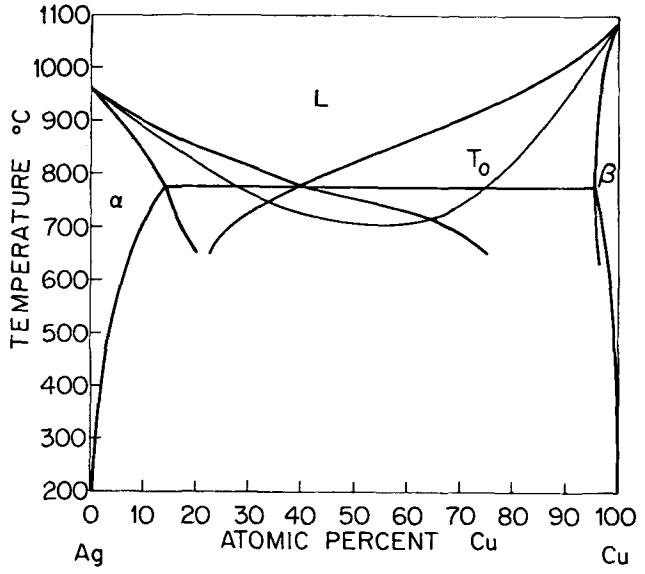

Fig. 13—Equilibrium Ag-Cu phase diagram (Ref. 13) showing calculated T_0 line and metastable liquidi and solidi lines, 650 °C < T < 779 °C.

containing both eutectic and metastable phase growth because the growth velocity is not uniform throughout the melt pool. It increases from zero at the bottom of the melt pool to the scan velocity on the center line at the back edge. It is possible that a nonequilibrium melt-α/β eutectic interface and a melt-γ interface might compete over a significant range of velocities.

It appears that a similar situation may exist in the Cu 37 at. pct Ag alloy. Close examination of the broad α and β peaks suggests that each peak results from the superposition of two closely spaced peaks. The α peak with the largest 2θ angle occurs at the same angle as the α' peak in the Cu 61.7 at. pct Ag alloy. Thus, it appears likely that regions of eutectic are also present in this alloy coating.

One possible explanation for the absence of γ in the coatings on the Cu 37 at. pct Ag and Cu 17 at. pct Ag alloys is that insufficient undercooling existed at the melt-solid interface. According to Figure 13, the maximum interface temperature at which γ can form in the Cu 37 at. pct Ag alloy is 715 °C. However, the metastable extended solid solution was observed in the Cu 82 at. pct Ag, Cu 71.8 at. pct Ag, and the Cu 61.7 at. pct Ag alloy trails indicating that melt-solid interface temperatures less than 838, 771, and 727 °C, respectively, were attained. In our previous investigation, we observed γ in single trails on Cu 50 at. pct Ag and Cu 25 at. pct Ag alloys both scanned at 10 cm s^{-1}, requiring melt-solid interface temperatures less than 708 and 779 °C, respectively. The 10 cm s^{-1} velocity should have produced less kinetic undercooling than that produced by the 34 cm s^{-1} scans in this investigation. Thus, insufficient undercooling appears to be an unlikely reason for the absence of γ in the Cu 37 at. pct Ag alloy. It is an even less likely reason for the absence of γ in the Cu 17 at. pct Ag alloy, where an interface temperature less than 880 °C is required.

Another explanation for the absence of γ in the Cu-rich alloys is difficulty in nucleation. This possibility is suggested by a previous observation that in laser melted trails regrowth occurs preferentially from the Ag-rich phase (see, for example, Figure 2, Reference 9). Either the γ phase nucleates more readily on the Ag-rich phase or this phase adjusts its composition during regrowth to become the same as γ. The laser pretreatment used in this investigation should have produced, however, a substrate consisting either of the metastable solid solution or a finely dispersed mixture of α and β phases. Thus, it does not appear that difficulty in nucleation is a likely explanation for the absence of γ in the Cu-rich alloys.

Still another explanation is that at the interface temperature determined by the scan velocity (34 cm s^{-1}), the melt-γ interface is slower than the melt-α/β interface. Boswell and Chadwick have compared growth rates for both interfaces and their results indicate that at interface temperatures only a few degrees less than the T_0 line the melt-γ interface should attain the highest velocity. In contrast, our results in the Cu 61.7 at. pct Ag and Cu 37 at. pct Ag alloys suggest that these interfaces compete over a significant range of velocities and interface temperatures. The probable source of this disagreement is the assumption that metastable equilibrium exists at the interface in the calculation of eutectic interface velocity. If our interpretation of the α' peak in the Cu 61.7 at. pct Ag alloy is correct, metastable equilibrium definitely does not exist.

Taking these various possibilities into account, we conclude that γ was probably formed from the melt in both the Cu 37 at. pct Ag and the Cu 17 at. pct Ag alloys. In the former alloy, some regions containing eutectic were also formed. Annealing, due to the melting of adjacent trails, caused the γ to transform to α and β. The α lattice parameter observed on the Cu-rich alloys is somewhat less than that observed in the Ag-rich alloys while the β lattice parameter is somewhat greater. This difference is attributed to a greater deviation from equilibrium in the Cu-rich alloys, probably due to lower transport rates.

B. *Banding*

The presence and regularity of compositional bands throughout the melt trails delineating sequential positions of the melt solid interface suggests that the occurrence of such bands may be explained on the basis of heat and mass transport at an undercooled planar interface. The coupled heat and mass flow differential equations can be written for such an interface; see, for example, Baker and Cahn.[12] The solution of these equations requires, however, a knowledge of conditions existing at the melt solid interface. For a binary system, these conditions are specified by two interface response functions:

$$f = f(C_S, C_L, T, V)$$
$$g = g(C_S, C_L, T, V)$$

where C_S = solid composition at interface
C_L = liquid composition at interface
T = interface temperature
V = interface velocity

Unfortunately, there is neither a theory predicting the form of these functions nor data from which they can be calculated for the far-from-equilibrium conditions of our experiments. Thus, it does not appear that solving the coupled heat and mass flow equations to obtain a detailed description of interface motion is possible at this time.

Thermodynamics gives some information regarding interface conditions for a binary system. It specifies that for a specific T, growth ($v > 0$) requires that C_S and C_L lie in certain composition ranges. These ranges are given for the

Ag-Cu system for three temperatures in Figure 14. The details of constructing such diagrams from the molar free energy curves of the melt and solid phases are described briefly in Appendix VI-B and in greater detail by Baker and Cahn.[12] The molar free energy *vs* composition curves used for the construction of Figure 14 are given in Appendix VI-B.

Consider, for example, solidification of the alloy with composition, Cu 62 at. pct Ag, where the interface temperature is 1052 K. The possible values of C_S and C_L at the interface are the locus of points lying inside or on the closed curve designated by the interface temperature. If solidification takes place at steady state, then C_S must equal Cu 62 at. pct Ag. Thus, for an interface temperature of 1052 K, steady state solidification of an alloy with composition Cu 62 at. pct Ag is not possible. If the interface temperature is decreased to 1003 K, then steady state solidification is possible for only one liquid composition, namely, $C_L = C_S = 38$ at. pct Cu. If the interface temperature is further decreased to 983 K, then a solid with composition Cu 62 at. pct Ag can form from melts ranging in composition from Cu 76 at. pct Ag to Cu 39 at. pct Ag. In this case, it is likely that a diffusion layer will be present in front of the interface and that the composition of the melt at the interface will not equal Cu 62 at. pct Ag.

An oscillation in interface composition can be shown as a closed curve; see arrows in Figure 14. If C_S becomes less than C_O, then conservation of mass requires that the melt must become enriched in solute. On the other hand, if C_S becomes greater than C_O, then the fraction of solute in the melt must decrease. If the melt composition at the interface approaches the limiting Cu-rich composition, a possible diffusional instability may arise, which was pointed out by Baker and Cahn.[12] A downward fluctuation in solid composition may cause the melt composition at the interface to move outside the range where steady state solidification is possible. In this case, the plane front interface would break down and lag back to a lower temperature. Such a mechanism may explain the apparent cellular breakdown observed in the eutectic melt trail (Figure 12).

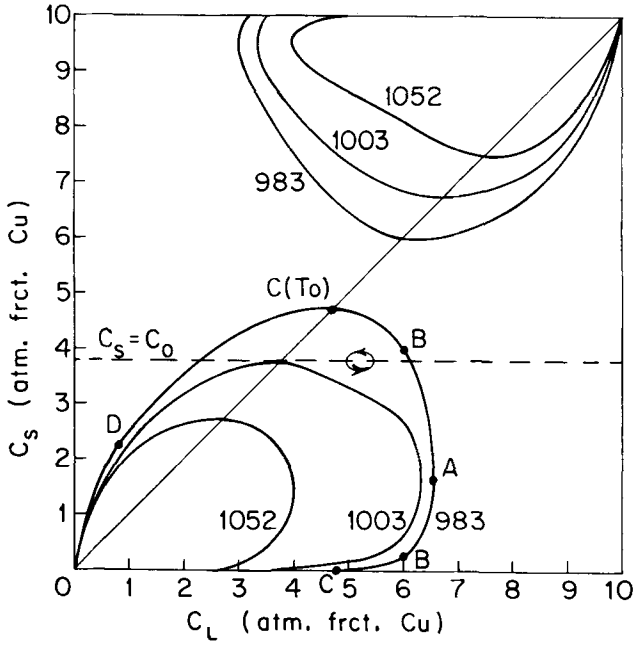

Fig. 14—The range of compositions that can form with a net decrease in free energy from a liquid of composition C_L. For steady-state solidification C_S must equal the alloy composition C_O. Thus, the diagram also gives the range of liquid compositions from which a solid of composition $C_S = C_O$ may form in steady-state solidification. The relationship of points A, B, C, C(T_0) and D to the ΔG_{MIX} *vs* composition curves for the solid and liquid phases is shown in Fig. 17, Appendix VI-B.

V. SUMMARY AND CONCLUSIONS

1. Coatings consisting of overlapping trails melted with a scanning CW CO_2 laser have been produced on Ag-Cu alloys with the following compositions: Cu 17 at. pct Ag; Cu 37 at. pct Ag; Cu 61.7 at. pct Ag; Cu 71.8 at. pct Ag; and Cu 82 at. pct Ag.
2. A metastable equilibrium diagram for Ag-Cu was constructed. The ΔG_{MIX} *vs* composition curve for the fcc solid solution phase was calculated from miscibility gap data using the Lumsden model. The ΔG_{MIX} *vs* composition curve for the liquid was calculated from an average of recent thermodynamic data.
3. Based on the calculated metastable equilibrium diagram and the observation of the metastable extended solid solution in the Cu 82 at. pct Ag, Cu 71.8 at. pct Ag, and Cu 61.7 at. pct Ag alloy trails, it is concluded that the melt-solid interface temperature must have been less than 838, 771, and 727 °C for these alloys, respectively, during solidification.
4. In addition to γ, the Ag-rich alloy trails were found to contain α. It is concluded that the α formed by precipitation during the annealing of melted and solidified trails by the subsequent melting of adjacent trails. Only a small amount of α was found in the Cu 71.8 at. pct Ag trail.
5. The Cu 61.7 at. pct Ag alloy trail also contained a phase α' with lattice parameter lying between α and γ. It is concluded that this phase is associated with eutectic regions.
6. No γ was detected in the Cu-rich compositions. It is concluded that γ was probably initially present but decomposed to α and β due to annealing during coating preparation.
7. Extensive banding corresponding to at least a 1 pct variation in composition was observed in the Cu 71.8 at. pct Ag and the Cu 61.7 at. pct Ag alloys. It is proposed that such banding is evidence for planar, oscillating, steady-state interface motion. The observation of repeated cellular breakdown of the planar interface in the Cu 61.7 at. pct Ag alloy is attributed to a diffusional instability previously proposed by Baker and Cahn.[12]

VI. APPENDIX

A. *Solidification Rate*

According to Tiller,[8] the minimum undercooling T_m is defined as:

$$T_m = \frac{4\sigma_{\alpha\beta} T_E}{L\,\lambda_m} \qquad [1]$$

with the parameters:

$\sigma_{\alpha\beta}$ = interphase boundary energy
= 0.2 J m^{-2}

T_E = eutectic temperature
= 1052 K
L = volumetric latent heat per mole for eutectic solidification of the α and β phases
= 1.95×10^9 J m^{-3}
λ_m = interlamellar spacing

For the eutectic alloy Cu 60.1 at. pct Ag, Cline and Lee have shown experimentally that $G\lambda_m^2 = 1.4 \times 10^{-17}$ m^{3}s^{-1} where G is the growth rate. We shall assume that this relation holds for coupled growth in Cu 50 at. pct Ag. Combining the above yields:

$$T_m = 115.35G^{1/2} \quad [2]$$

Figure 1 is a plot of growth rate, G, *vs* melt temperature.

B. T_0-Line and Metastable Solvus and Liquidus Lines

In order to determine the T_0-line and metastable solvus and liquidus lines for the Ag-rich and Cu-rich terminal solid solutions, it is necessary to calculate ΔG_{MIX} for the solid and liquid phases. The T_0-line is then determined by noting for a particular temperature the composition where the two ΔG_{MIX} curves cross. The metastable solvus and liquidus lines are determined by noting for a particular temperature the compositions of the intersection points of the common tangent to the ΔG_{MIX} curves.

Sundquist has evaluated various methods based on solution models for obtaining free energies of mixing from miscibility gap data.[11] The solution model developed by Lumsden[10] was found to give results often in excellent agreement with experiments. In the case of Ag-Cu, excellent agreement was obtained between the predicted ΔG_{MIX} curve for the solid phase and that determined by experiment.

Following Sundquist, we write ΔG_{MIX} for a two-component system in the form

$$\Delta G_{MIX} = N_1N_2f(N_i,T) + RT(N_1 \ln N_1 + N_2 \ln N_2) \quad [3]$$

For the solid fcc phase, we set

$$f(N_i,T) = \frac{C_1}{N_1 + r^2N_2} + \frac{C_2}{N_1 + r^5N_2} - N_1N_2\frac{C_1^2}{ZRT(N_1 + r^{8/3}N_2)^3} \quad [4]$$

where C_1 and C_2 are two parameters to be determined, r is the ratio of the atomic radius of component 2 to component 1, and Z is the coordination number of atoms in the solution.

Equations [3] and [4] describe the solution model developed by Lumsden. The parameters C_1 and C_2 are calculated from the solubility limits N_2' and N_2'' for a particular temperature. We may derive two equations in two unknowns, C_1 and C_2, that are quadratic in C_1 by setting the chemical potentials $\mu_1(N_2') = \mu_1(N_2'')$ and $\mu_2(N_2') = \mu_2(N_2'')$. They may be solved by: (i) solving one equation for C_2 in terms of C_1; (ii) substituting this result into the other equation; and, (iii) solving the resulting quadratic equation for C_1. Following this procedure, setting $N_2 = N_{Cu}$, $r = 0.889$ and, as recommended by Sundquist, $Z = 7$, we obtain results given in Table III.

To calculate the ΔG_{MIX} *vs* composition curve for the liquid, the ideal entropy of mixing was added to values of ΔG_{XS} obtained by averaging the results of five recent investigations, which were in good agreement.[14-18] The average values calculated for ΔG_{XS} are listed in Table IV. To relate the liquid and solid ΔG_{MIX} curves, the quantity $(1-N_{Cu})\Delta G_f(Ag) + N_{Cu}\Delta G_f(Cu)$ was added to the calculated ΔG_{MIX} values for the liquid. The free energy of fusion, ΔG_f, of each pure metal was obtained from the relation

$$\Delta G_f = \Delta H_f\left(\frac{T_f - T}{T_f}\right) \quad [5]$$

where ΔH_f is the enthalpy of fusion and T_f is the melting temperature.[19] The following values were used: for Cu, T_M = 1356 K and ΔH_f = 3120 cal mol^{-1}; and for Ag, T_M = 1234 K and ΔH_f = 2700 cal mol^{-1}.[20]

Curves for ΔG_{MIX} *vs* composition are given for 1052, 1003, and 983 K in Figures 15 to 17, respectively. At the eutectic temperature (1052 K) the liquid and solid ΔG_{MIX} *vs* composition curves should share a common tangent. The contact point of the liquid curve and the common tangent should occur at the eutectic composition (Cu 60.1 at. pct Ag). An examination of Figure 15 shows that the liquid and solid curves do share a common tangent which contacts the liquid curve at the eutectic composition. This excellent agreement is a basis for confidence in Lumsden model, the ΔG_{XS} *vs* composition data for the liquid, and the validity of the approximation used in deriving Eq. [5], *i.e.*, that the difference in specific heat between the solid and liquid phases is negligible.

In Figure 16 we have identified the intersections of the solid and liquid ΔG_{MIX} curves used to establish the T_0 compositions at 1003 K ($N'_{Cu}(T_0)$ and $N''_{Cu}(T_0)$ in Table V; see also Figure 13). Also shown are the common tangents used to establish the metastable solidi ($N'_{Cu}(S)$ and $N''_{Cu}(S)$ in Table V; see also Figure 13) and liquidi ($N'_{Cu}(L)$ *and* $N''_{Cu}(L)$ in Table V; see also Figure 13).

Table III. Parameters Used in Calculating ΔG_{MIX} for Solid Phase

	Miscibility Limits[13]		Lumsden Parameters	
T(°K)	N'_{Cu}	N''_{Cu}	C_1	C_2
1052	0.141	0.951	4656.6	789.9
1023	0.118	0.961	4679.0	839.7
1003	0.106	0.966	4680.4	867.9
993	0.102	0.968	4623.0	913.0
983	0.095	0.970	4744.7	845.2
973	0.091	0.971	4814.6	785.8
963	0.088	0.973	4687.1	884.0
948	0.082	0.976	4572.7	990.4
923	0.072	0.980	4508.9	1071.5
898	0.064	0.982	4661.5	942.1

Table IV. Average Values for ΔG_{XS} *vs* Composition for Liquid Ag-Cu Alloys

N_{Cu} (pct)	0	0.1	0.2	0.3	0.4	0.5	0.6	0.7	0.8	0.9	1.0
ΔG_{XS} (cal mol^{-1})	0	264	487	674	732	771	741	651	511	305	0

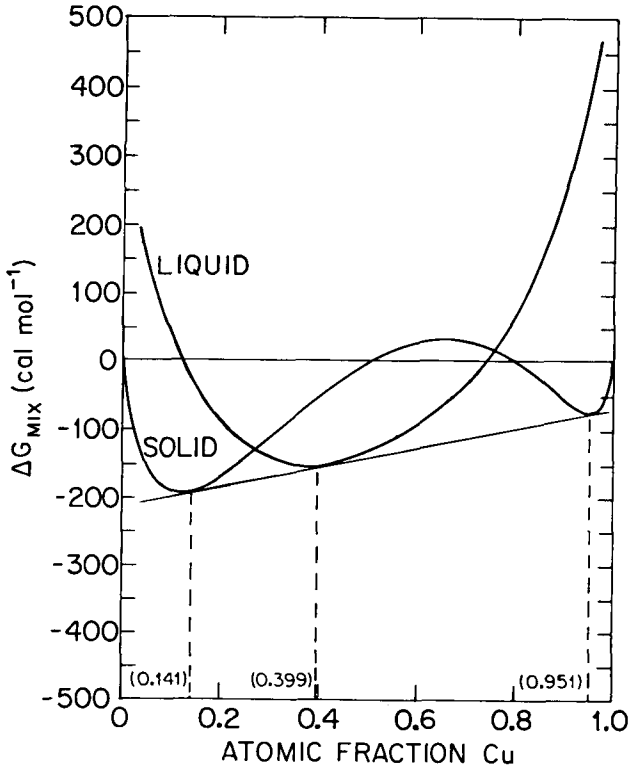

Fig. 15—The ΔG_{MIX} *vs* composition curves for liquid and solid phases at 1052 K. The common tangent construction correctly predicting the composition of α, β, and liquid is shown.

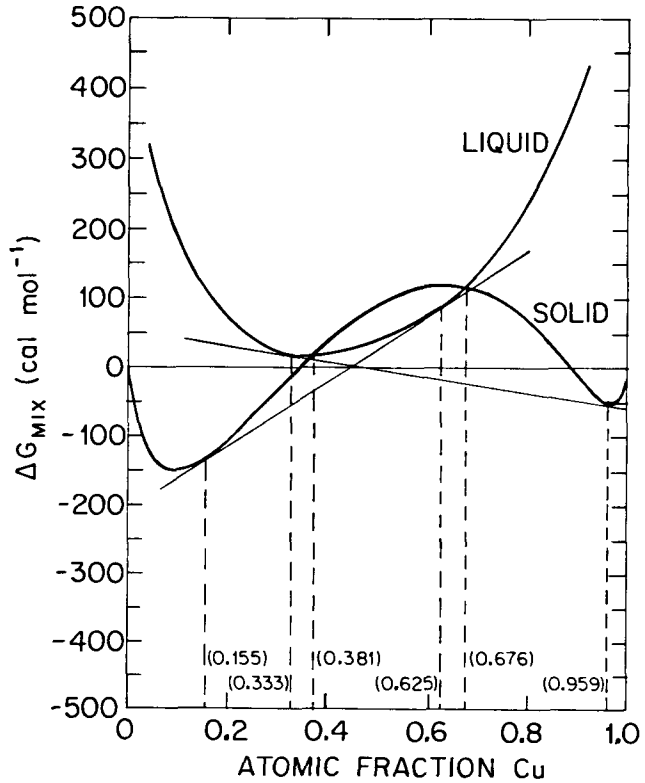

Fig. 16—The ΔG_{MIX} *vs* composition curves for liquid and solid phases at 1003 K. The common tangent construction for predicting metastable solidi and liquidi is shown. The T_0 line compositions correspond to the intersection points of the 2 curves.

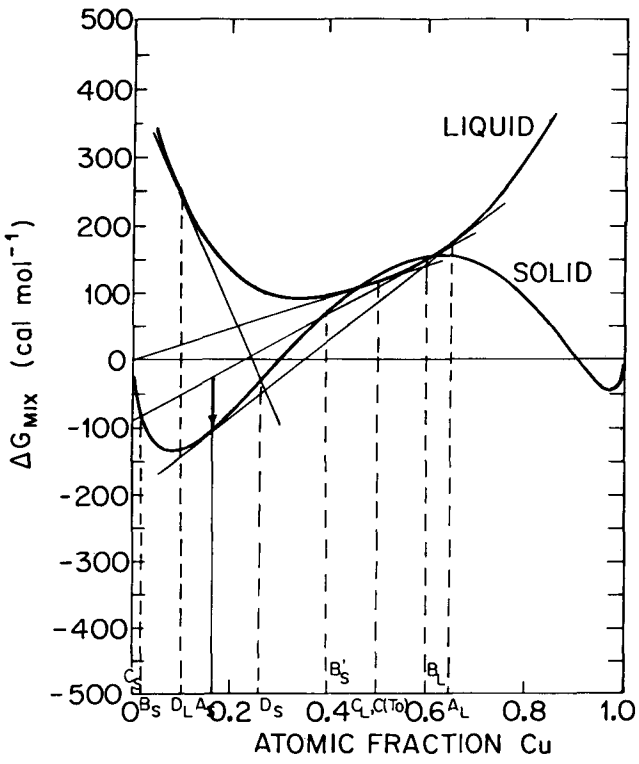

Fig. 17—The ΔG_{MIX} *vs* composition curves for liquid and solid phases at 983 K. The tangent to curve construction used to draw Fig. 14 is illustrated.

In Figure 17 we have shown the tangent-to-curve constructions for the Ag-rich solid phase used to draw Figure 14, which shows the range of solid compositions that can form with a net decrease in free energy from a specific liquid composition. This construction is based on the rule that the free energy change associated with transferring a small amount of material from the liquid phase, *e.g.*, composition B_L to the solid phase, *e.g.*, composition A_S, is given by the vertical arrow shown in Figure 17 from the tangent that contacts the liquid ΔG_{MIX} curve at B_L to the solid ΔG_{MIX} curve at A_S. It follows that there is a negative free energy change associated with transferring a small amount of material from a liquid phase of composition B_L to solid phases ranging in composition from B_S to B_S' which is the result indicated by Figure 14. In the case of the C(T_0) point in Figure 14, the tangent-to-curve rule becomes a curve-to-curve rule. Composition values corresponding to points A, B, C, C(T_0), and D in Figure 14 are indicated in Figure 17. Values for $N_{Cu}(T_0)$ and the metastable solidi and liquidi based on ΔG_{MIX} curves for the solid and liquid are listed in Table V.

Table V. Values Describing T_0-Line and Metastable Solidi and Liquidi. The Primed Values Are the Ag-Rich Values, and the Double Primed Values Are the Cu-Rich Values.

T(°K)	$N'_{Cu}(T_0)$	$N''_{Cu}(T_0)$	$N'_{Cu}(S)$	$N''_{Cu}(S)$	$N'_{Cu}(L)$	$N''_{Cu}(L)$
1052	0.275	0.750	0.141	0.951	0.399	0.399
1023	0.326	0.714	0.148	0.962	0.348	0.548
1003	0.381	0.676	0.155	0.959	0.333	0.625
993	0.432	0.647	0.155	0.965	0.322	0.641
983	0.478	0.600	0.165	0.962	0.300	0.658
973	—	—	0.171	0.959	0.258	0.675
923	—	—	0.200	0.969	0.235	0.750

ACKNOWLEDGMENTS

The authors wish to thank Professor John Perepezko, University of Wisconsin-Madison, for helpful suggestions regarding the estimation of ΔG_{MIX} for the liquid phase. We also are pleased to acknowledge support of this research by the National Science Foundation, Metallurgy Program, Grant No. DMR 78-07532.

REFERENCES

1. P. Duwez, R. H. Willens, and W. Klement, Jr.: *J. Appl. Phys.*, 1960, vol. 31, pp. 1136-37.
2. R. K. Linde: *J. Appl. Phys.*, 1966, vol. 37, p. 934.
3. R. Stoering and H. Conrad: *Acta Met.*, 1969, vol. 17, p. 933.
4. S. Nagakura, S. Toyama, and S. Oketani: *Acta Met.*, 1966, vol. 14, p. 73.
5. B. Predel and G. Schluckebier: *Z. Metallk.*, 1972, vol. 63, p. 782.
6. P. G. Boswell and G. A. Chadwick: *J. Mat. Sci.*, 1977, vol. 12, pp. 1879-94.
7. W. A. Elliot, F. P. Gagliano, and G. Krauss: *Metall. Trans.*, 1973, vol. 4, pp. 2031-37.
8. W. A. Tiller: *Liquid Metals and Solidification*, ASM, Metals Park, OH, 1958, p. 276.
9. David G. Beck, S. M. Copley, and M. Bass: *Metall. Trans. A*, 1981, vol. 12A, pp. 1687-92.
10. John Lumsden: *Thermodynamics of Alloys*, The Institute of Metals, London, 1952, p. 335.
11. B. E. Sundquist: *Trans. TMS-AIME*, 1966, vol. 236, pp. 1111-22.
12. James C. Baker and John W. Cahn: *Solidification*, ASM, Metals Park, OH, 1971, pp. 23-58.
13. M. Hansen and K. Anderko: *Constitution of Binary Alloys*, McGraw-Hill Book Co., New York, NY, 1958, p.18.
14. J. Golonka, J. Botor, and M. Dulat: *Metals Tech.*, July 1979, pp. 267-72.
15. J. Golonka: *Arch. Hutn.*, 1965, vol. 10, p.144.
16. S. Nakamura, T. Yawaji, and E. Kato: *Metall. Trans.*, 1970, vol. 1, p. 2645.
17. S. Wagner: *High Temp. Sci.*, 1971, vol. 3, p. 481.
18. U. V. Choudary and A. Ghosh: *J. Electrochem. Soc.*, 1970, vol. 117, p. 1024.
19. David R. Gaskell: *Introduction to Metallurgical Thermodynamics*, McGraw-Hill Book Co., New York, NY, 1981.
20. D. R. Stull and G. C. Sinke: *Thermodynamic Properties of the Elements*, American Chemical Society, Washington, DC, 1956.